Control of tonal noise from subsonic axial fan. Part 1: reconstruction of aeroacoustic sources from far-field sound pressure

Anthony Gérard, Alain Berry*, Patrice Masson

G.A.U.S., Mechanical Engineering Department, Université de Sherbrooke, 2500 blvd Université, Sherbrooke, Que., Canada J1K 2R1

Abstract

An inverse method is investigated to evaluate the unsteady rotating forces (dipole strength distribution) acting by the fan on the fluid from far-field acoustic pressure measurements. A development based on the tonal noise generated by a propeller is used to derive a discretized form of the direct problem. The inversion of this direct problem is ill-posed and requires optimization technique to stabilize the solution for small perturbations in the measured acoustic input data. The reconstruction reveals that the conditioning of the inverse model depends on the aeroacoustic source and far-field sensor locations as well as on the frequency under investigation. Simulations show that an adequate choice of a regularization parameter leads to a satisfactory reconstruction of imposed unsteady rotating forces in the presence of measurement noise, and a correct localization of acoustic "hot spots" on the radiation surface. Preliminary experimental results also show the ability to extrapolate the radiated sound field at blade passage frequency (BPF), and harmonics, from the reconstructed forces. These data are exploited in the second part of this paper to evaluate various active control strategies for tonal fan noise.

*Corresponding author. Tel.: +1 819 821 8000x2148; fax: +1 819 821 7163.
  E-mail address: alain.berry@usherbrooke.ca (A. Berry).

Nomenclature

a_1	inner rotor radius
a_2	outer rotor radius
B	number of blades
c	speed of sound
$\mathbf{e}$	error vector
f_z	axial pressure component acting on the rotor
f_z^0	time average value of the axial pressure
$\bar{f}_z^0$	circumferential average value of f_z^0
g_{1z}	Green function (dipolar radiation along the z axis)
$\mathbf{H}_s$	transfer function matrix at $\omega = s\omega_1$
i	imaginary number ($\sqrt{-1}$)
I	number of radial elements
J	number of point in the discretized radiation space
J_s	cost function at $\omega = s\omega_1$
J_{sb+q}	Bessel function of the $(sB + q)$th order
k	wavenumber ($k = sk_1 = s\omega_1/c$ with $\omega_1 = B\Omega$)
p	acoustic pressure
p_s	acoustic pressure at $s\omega_1$
$\hat{\mathbf{p}}_s$	far-field acoustic pressure measurement vector at $s\omega_1$
q_{min}, q_{max}	minimum and maximum circumferential order q to be reconstructed
Q	number of circumferential harmonics to be reconstructed
S/N	signal-to-noise ratio
r, φ, ϑ	spherical coordinates in the radiation space
x, y, z	Cartesian coordinates in the radiation space

r_1, φ_1	polar coordinates in the rotor plane
t	time
α_s	time Fourier coefficient
β	regularization parameter
β_q	Azimuthal Fourier coefficient
Δr_1	distance between two radial elements
κ	condition number
σ^2	variance of the random error vector added to the simulated sound pressures
σ_i	singular values
ω	angular frequency
ω_1	blade passage angular frequency ($\omega_1 = B\Omega$)
Ω	angular velocity of the rotor

Subscripts and indices

q, l	circumferential index
s, n	frequency index
i	radial element
j	radiation space discretization index
L	condensed source discretization index (i, q)
z	axial component
φ	radial component

Superscripts

H	Hermitian
∗	complex conjugate
+	pseudo-inverse

1. Introduction

Due to the increasing demand of improved passenger safety and comfort and to the increasing use of communication systems, interior acoustic comfort of future automobiles is expected to be one of the main decision-making factors in an extremely competitive market. Tonal noise of axial engine cooling fans is among the several noise sources inside an automobile. For fans with equal blade pitch, dominant tones are radiated underhood by engine cooling fans at the blade passing

frequency (BPF, typically around 300 Hz) and its multiples, and are transmitted in the car interior. Therefore, there is a need for manufacturers of engine cooling units to design improved, low-noise axial fans. These two companion papers investigate active control of tonal noise from axial automotive fans as a solution to increase interior acoustic comfort of cars. The first part details an inverse aeroacoustic model to characterize an automotive axial fan as an extended acoustic source; the second part exploits this aeroacoustic model in active control simulations and experiments in free field.

Fan noise has been a topic of research since the first analytical aeroacoustic models by Ffowcs Williams and Hawkings [1], Wright [2] or Lowson [3] some 30 years ago. Direct methods have been developed for the calculation of the radiated sound field based on the dynamic forces applied by the blades on the fluid in a fixed reference frame. Rotor tonal noise resulting from vane/rotor interaction or non-uniform flow conditions has been extensively studied [2–4], and it has been demonstrated that, at a rotation Mach number below 0.8 [5], the quadrupolar source can be neglected and the unsteady pressure along the blade surface is equivalent to a dipole distribution. However, it is difficult in practice to estimate the strength of this extended acoustic source. State-of-the-art CFD or aeroacoutic codes presently attempt to predict the unsteady aerodynamics and both the tonal and broadband sound radiation of the propeller [6]; on the other hand, the measurement of pressure fluctuations on the fan blades require sophisticated or expensive experimental techniques such as integrated piezoplastic sensors [7] or other miniature pressure transducers [8].

Alternative inverse aeroacoustic problems have been recently investigated to overcome these difficulties and to develop non-contact measurement techniques. For example, Li and Zhou [9] developed an inverse method to reconstruct the blade surface pressure distribution from the radiated sound field. Their work is based on the inversion of the Farassat integral solution of the Ffowcs Williams and Hawkings equation, assuming that the aerodynamic loading on the surface of the propeller is steady. Luo and Li [10] also proposed an inverse aeroacoustic model of rotor wake/stator interaction based on a Fredholm integral equation of the first kind. The unsteady surface distribution on the stator surface is derived from the radiated sound field. Other studies focused on the inverse aeroacoustic model of a rectangular wing or a flat plate interacting with a gust [11,16]. The above inverse aeroacoustic models generally lead to the inversion of an ill-conditioned matrix. Numerical results demonstrate that optimization and regularization techniques have been successfully used to solve these problems [12] but no experimental results have been reported yet for the source characterization of axial fans.

This paper investigates an inverse aeroacoustic approach to model the elementary acoustic source distribution on the surface of an axial fan from its far-field noise directivity. The derivation of an accurate and physically realistic acoustic model of an axial fan is the first step towards an effective active noise control strategy. The proposed inverse model takes into account the flow disturbance responsible for the tonal noise generation of subsonic axial fans. In the first section of the paper, the direct aeroacoustic model is detailed, whereby the far-field radiated sound is related to the non-uniform flow and the blade pressure distribution by solving the Helmholtz integral following the approach of Morse and Ingard [4]. The inverse model is detailed in the following section, and a regularization technique is proposed to overcome a poor conditioning of the inverse problem. The inversion is first tested on simple examples to assess the influence of a number of parameters (such as the discretization of the fan source, frequency and sensing configuration) on

the conditioning of the inverse model. Then, a numerical case related to non-uniform upstream flow condition is conducted to demonstrate the feasibility of the reconstruction approach and the ability to distinguish the acoustically radiating components obtained from flow non-uniformities. Finally, preliminary experimental results for the extrapolation of the radiated sound field at blade passage frequency (BPF) and at its harmonics are presented on an actual engine cooling system.

2. A direct model for tonal noise of subsonic axial fans

The general aeroacoustic equations derived by Ffowcs Williams and Hawkings (FW–K) [1] include the case of a moving surface in an infinite fluid medium at rest outside the flow region [5], and therefore can be used to extract the physical mechanisms of axial fan noise. In general, the expression of the acoustic pressure in the fluid involves three terms: the first term is associated with a moving quadripole source that represents the generation of sound due to turbulent volume sources and corresponds to the solution of the Lighthill theory. This quadripole source is significant only if the blade tip Mach number exceeds 0.8 [5] and is therefore irrelevant to the automotive fan noise, for which blade tip Mach numbers generally do not exceed 0.15. The second term is related to a moving dipole source due to the unsteady forces exerted by the solid surfaces on the fluid. This is the well-known 'loading noise' or 'dipole noise', the principal cause of fan noise [2,5]. The last term is equivalent to a monopole radiation due to the volume displacement effects of the moving surfaces, also called 'thickness noise'. The efficiency of thickness noise is poor at low fan rotation speed since the circumferential phase velocity of the fluid pressure fluctuations generated by the moving blades is well below sonic velocity [13]. Therefore, the main source term for subsonic axial fans is the distribution of forces applied by the blades on the fluid. Periodic forces (steady rotating forces or unsteady rotating forces due to non-uniform but stationary upstream flow) lead to discrete tones generation while random forces (such as turbulent boundary forces) lead to broadband noise.

This section focuses primarily on the discrete tone generation at the BPF and its multiples due to non-uniform, stationary upstream flow field. Indeed, when the flow entering the fan is uniform, the blade forces are steady in a coordinate system rotating with the propeller, but they have an angular frequency equal to $\omega_1 = B\Omega$ in a fixed reference frame (Ω is the angular velocity of the fan and B is the number of blades, assuming an equal blade pitch). For subsonic fans, the circumferential velocity of these forces is below the sound speed, thus this source (first derived by Gutin) does not radiate efficiently. However, even a slight flow irregularity (non-uniform flow) causes circumferentially varying blade forces and gives rise to a considerably larger radiated sound at the BPF and its harmonics, especially in the axial direction of the fan [4]. In many instances, axial fans operate in a non-uniform flow: this is the case of engine cooling axial fans that operate behind a radiator/condenser system or in the wake of inlet guide vanes. The interactions between the flow and the blades can be classified into potential interactions and wake interactions [5].

There are many theoretical investigations of the radiated acoustic pressure as a function of the fluctuating forces exerted by the rotating blades on the fluid [2–5], assuming that these forces can be mathematically modelled or experimentally measured. We chose to use the direct fan noise model of Morse and Ingard [4] because it leads to explicit analytical solutions of the radiated

sound field. In this model, Morse and Ingard directly postulate the forces into the spectral domain (circumferential Fourier series decomposition) and introduce these forces as dipolar source terms in the Helmholtz equation to derive the radiated sound field [4]. In contrast, the FW–H theory introduces the force source terms in the spatial domain using a retarded time formulation [5]. Moreover, Fowcs Williams and Hawkings derived their equation by extending the Lighthill acoustic analogy to include the effects of solid boundary surfaces. As opposed to this, Morse and Ingard directly assumed that the force distribution on a surface generates a dipolar-like sound field and can be calculated by introducing them into the Helmholtz integral. Thus, the Morse and Ingard model should be seen as capable of predicting "*the sound field produced by a source distribution which, in its essentials, could serve as a model for a propeller*" [4]. In spite of these differences, both approaches lead to qualitatively very similar expressions of the sound radiation.

The system under study and coordinate systems are depicted in Fig. 1. Polar coordinates (r_1, φ_1) are used to specify a point on the fan area, and spherical coordinates (r, φ, θ) or Cartesian coordinates (x, y, z) are used to specify a point in the acoustic domain. The main derivations of the Morse and Ingard model are recalled in this section. The first step of the direct model is to obtain the aerodynamic forces per unit area at (r_1, φ_1) acting on the rotor blades for a non-uniform flow passing through the fan. The second step derives the acoustic radiation of the corresponding elementary dipoles at the BPF and its harmonics at (r, φ, θ).

2.1. Case of uniform flow

The aerodynamic pressure exerted by the fan blades on the fluid are decomposed into an axial (z) component related to the thrust and a circumferential component related to the drag. The pressure is assumed to be zero in the area between the blades. In a uniform flow, the fluid pressure in a fixed reference frame is periodic in time with an angular frequency $\omega_1 = B\Omega$, with its amplitude independent of φ_1 and its phase proportional to φ_1. Thus, the time Fourier series of the axial component of the aerodynamic pressure can be written as

$$f_z(t; r_1, \varphi_1) = \sum_{s=-\infty}^{+\infty} A_s(r_1) e^{-is\omega_1(t - \varphi_1/\Omega)} = f_z^0(r_1) \sum_{s=-\infty}^{+\infty} \alpha_s(r_1) e^{isB\varphi_1} e^{-is\omega_1 t} \qquad (1)$$
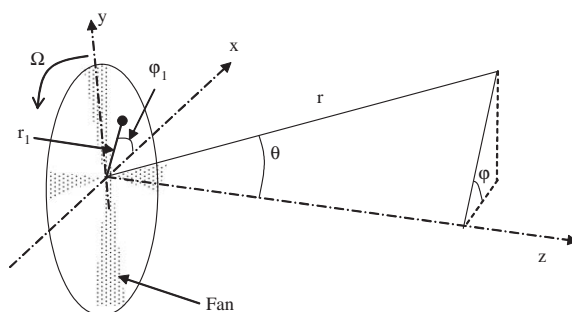

Fig. 1. Sound radiation from an axial fan (coordinate systems).

with

$$\alpha_s(r_1) = \frac{A_s(r_1)}{f_z^0(r_1)}, \quad i = \sqrt{-1}$$

and t is the time. In Eq. (1), $\alpha_s(r_1)$ is the coefficient of the Fourier series of the axial pressure in the time domain, representing the complex strength of the sth harmonic of the BPF and $f_z^0(r_1)$ is the time average value of the axial force per unit area at the radial position r_1. In the following, the circumferential component of the aerodynamic pressure (related to aerodynamic drag on the blades) will be neglected in comparison to the axial aerodynamic pressure (z component) since this is usually the case for a well-designed propeller.

2.2. Case of non-uniform flow

In the case of a circumferentially varying (but stationary) flow, the time average axial force per unit area f_z^0 is now a function of both r_1 and φ_1. This force can itself be expanded into a spatial Fourier series over the circumferential coordinate

$$f_z^0(r_1, \varphi_1) = \bar{f}_z^0(r_1) \sum_{q=-\infty}^{q=+\infty} \beta_q(r_1) e^{iq\varphi_1}, \tag{2}$$

where β_q is the Fourier coefficient of the qth circumferential harmonic that accounts for the non-uniformity with respect to φ_1, and $\bar{f}_z^0(r_1)$ is the circumferential average of $f_z^0(r_1, \varphi_1)$ at the radial position r_1. Even if the circumferential variation of the upstream flow is small, it generally leads to considerably larger radiated sound at low Mach number [4,14]. In the case of non-uniform flow, the expression of the fluctuating axial pressure is therefore

$$f_z(t; r_1, \varphi_1) = \bar{f}_z^0(r_1) \sum_{s=-\infty}^{+\infty} \sum_{q=-\infty}^{+\infty} \alpha_s(r_1) \beta_q(r_1) e^{i(sB+q)\varphi_1} e^{-is\omega_1 t}. \tag{3}$$

2.3. Free field acoustic radiation

The axial fluctuating blade forces appear as dipole terms in the Helmholtz radiation integral, so the acoustic pressure can be expressed by integrating the unsteady rotating forces over the fan area A,

$$p(t; r, \varphi, \vartheta) = \iint_A f_z(t; r_1, \varphi_1) g_{1z}(t; r_1, \varphi_1; r, \vartheta, \varphi) r_1 \, dr_1 \, d\varphi_1, \tag{4}$$

where g_{1z} is the sound field from a unit strength point force in the z direction at (r_1, φ_1). Following Morse and Ingard [4], a far-field ($r \gg r_1$) approximation of g_{1z} is given by

$$g_{1z} = -ik \cos\vartheta \frac{e^{ikr}}{4\pi r} \sum_{m=-\infty}^{+\infty} i^m J_m(kr_1 \sin\vartheta) e^{im(\varphi-\varphi_1)} e^{-i\omega t}, \tag{5}$$

where $k = \omega/c$ is the acoustic wavenumber, c is the sound speed, ω is the angular frequency of the radiated sound and J_m is the cylindrical Bessel function of order m. In order to express the

resulting far-field radiation of the fan at the multiples of the BPF, one must substitute Eqs. (3) and (5) into Eq. (4) and set $\omega = s\omega_1$ and $k = s\omega_1/c = sk_1$. Solving for the Helmholtz integral, and using the orthogonality relations

$$\int_0^{2\pi} e^{i(sB+q)\varphi_1} e^{-im\varphi_1}\, d\varphi_1 = 2\pi \quad \text{if } sB+q = m$$

and

$$\int_0^{2\pi} e^{i(sB+q)\varphi_1} e^{-im\varphi_1}\, d\varphi_1 = 0 \quad \text{if } sB+q \neq m,$$

the acoustic radiation due to axial forces is finally given by

$$p(t; r, \varphi, \vartheta) = -\frac{ik_1 \cos\vartheta}{4\pi r} \sum_{s=-\infty}^{+\infty} \sum_{q=-\infty}^{+\infty} i^{sB+q} e^{isk_1 r} e^{i(sB+q)\varphi - is\omega_1 t}$$

$$\times \int_{a_1}^{a_2} s\bar{f}_z^0(r_1)\alpha_s(r_1)\beta_q(r_1) J_{sB+q}(sk_1 r_1 \sin\vartheta) 2\pi r_1\, dr_1. \tag{6}$$

In Eq. (6), s and q represent the Fourier series expansions of the dipole strength over time t and over the circumferential coordinate φ_1, respectively. Moreover, a_1 and a_2 are the interior radius and exterior radius of the fan, respectively.

Morse and Ingard [4] proposed the following alternative form of Eq. (6):

$$p(t; r, \vartheta, \varphi) = \frac{\cos\vartheta}{r} \sum_{n=1}^{+\infty} (nk_1)$$

$$\times \left\{ \sum_{l=0}^{+\infty} \int_{a_1}^{a_2} \bar{f}_z^0(r_1)\alpha_n(r_1)\beta_l(r_1) J_{nB-l}(nk_1 r_1 \sin\vartheta) \right.$$

$$\times \sin\left[nk_1(r-ct) + (nB-l)\left(\varphi + \frac{\pi}{2}\right) \right] r_1\, dr_1$$

$$+ \sum_{l=0}^{+\infty} \int_{a_1}^{a_2} \bar{f}_z^0(r_1)\alpha_n(r_1)\beta_l(r_1) J_{nB+l}(nk_1 r_1 \sin\vartheta)$$

$$\left. \times \sin\left[nk_1(r-ct) + (nB+l)\left(\varphi + \frac{\pi}{2}\right) \right] r_1\, dr_1 \right\}, \tag{7}$$

where n and l are indices, respectively, accounting for time Fourier series decomposition and circumferential Fourier series decomposition.

It can be seen from Eq. (7) that the radiated sound field can be decomposed into two groups of progressing waves. The first group involves Bessel functions of order $nB-l$, which corresponds to a rapidly rotating source pattern; the associated acoustic pressure field rotates with an angular velocity

$$\omega_- = \frac{n\omega_1}{nB-l} = \frac{nB}{nB-l}\,\Omega$$

which is larger than Ω. The second group of waves involves Bessel functions of order $nB + l$, which corresponds to a slowly rotating source pattern; the acoustic pressure field rotates with an angular velocity

$$\omega_+ = \frac{n\omega_1}{nB + l} = \frac{nB}{nB + l}\,\Omega$$

which is smaller than Ω. For all values of nB, the J_{nB-l} terms are much larger than the J_{nB+l} terms, provided that the argument $nk_1r_1 \sin\vartheta$ is roughly smaller than 1. In this case, the second group of waves is therefore an inefficient noise radiator and can be neglected. Thus, Eq. (7) can be suitably approximated by

$$
\begin{aligned}
p(t; r, \vartheta, \varphi) = \frac{\cos\vartheta}{r} \sum_{n=1}^{+\infty} (nk_1) \\
\times \sum_{l=0}^{+\infty} \int_{a_1}^{a_2} \bar{f}_z^0(r_1)\alpha_n(r_1)\beta_l(r_1)J_{nB-l}(nk_1r_1 \sin\vartheta) \sin\left[nk_1(r - ct)\right. \\
\left. +(nB - l)\left(\varphi + \frac{\pi}{2}\right)\right] r_1 \, dr_1.
\end{aligned}
\tag{8}
$$

It can also be noted that the case $l = nB$ generally has a large contribution in the sum and results in a $J_0(nk_1r_1 \sin\vartheta)$ directivity function, which has its maximum along the fan axis ($\vartheta = 0$). In such a case, all the elementary radiating dipoles fluctuate in phase (the theoretical wave speed is infinite) and the directivity of the sound radiation is a dipole along the fan axis. In practice, the sound pressure must be computed with Eq. (8) by summing the circumferential Fourier coefficients l around the value nB for a particular multiple n of the BPF.

The analytical results derived in this section are consistent with those derived by Lowson [3], Goldstein [5] or by Blake [17]. The models are qualitatively equivalent except for the definition of the source terms.

3. Inverse model

3.1. Discretizing the direct model

In the following, Eq. (6) is written in terms of a time harmonic expansion:

$$p(t; r, \varphi, \vartheta) = \sum_{s=-\infty}^{s=+\infty} p_s(s\omega_1; r, \varphi, \vartheta)e^{-is\omega_1 t} \tag{9}$$

with

$$
\begin{aligned}
p_s(s\omega_1; r, \varphi, \vartheta) = -\frac{ik_1 \cos\vartheta}{4\pi r} \sum_{q=-\infty}^{+\infty} i^{sB+q}e^{isk_1r}e^{i(sB+q)\varphi} \\
\times \int_{a_1}^{a_2} s\bar{f}_z^0(r_1)\alpha_s(r_1)\beta_q(r_1)J_{sB+q}(sk_1r_1 \sin\vartheta)2\pi r_1 \, dr_1.
\end{aligned}
\tag{10}
$$

Discretizing the integral over r_1 and truncating the sum over the circumferential harmonics q in Eq. (10) leads to

$$p_s(s\omega_1; r, \varphi, \vartheta) = -\frac{ik_1 \cos \vartheta}{4\pi r_j} \sum_{q=q_{min}}^{q=q_{max}} i^{sB+q} e^{isk_1 r} e^{i(sB+q)\varphi}$$

$$\times \sum_{i=1}^{I} s\bar{f}_z^0(r_{1i})\alpha_s(r_{1i})\beta_q(r_{1i}) J_{sB+q}(sk_1 r_{1i} \sin \vartheta_j) 2\pi r_{1i} \Delta r_1, \tag{11}$$

where r_{1i} are I equally spaced points in the interval $[a_1 a_2]$ separated by Δr_1 and q_{min}, q_{max} are the minimal and maximal circumferential harmonics in the sum; in the calculation of Eq. (11), q_{min}, q_{max} are chosen such that $q_{min} < -sB < q_{max}$. Finally, we introduce the index j to discretize the radiation space into J locations $p_{sj} = p_s(s\omega_1; r_j, \varphi_j, \vartheta_j)$,

$$p_{sj} = -\frac{ik_1 \cos \vartheta_j}{4\pi r} \sum_{q=q_{min}}^{q=q_{max}} i^{sB+q} e^{isk_1 r_j} e^{i(sB+q)\varphi_j}$$

$$\times \sum_{i=1}^{I} s\bar{f}_z^0(r_{1i})\alpha_s(r_{1i})\beta_q(r_{1i}) J_{sB+q}(sk_1 r_{1i} \sin \vartheta) 2\pi r_{1i} \Delta r_1. \tag{12}$$

Eq. (12) can be written in a compact form

$$p_{sj} = \sum_L H_{sjL} f_{sL}, \tag{13}$$

where the i and q indices have been condensed into a single index $L = (i, q)$, $f_{sL} = \bar{f}_z^0(r_{1i})\alpha_s(r_{1i})\beta_q(r_{1i})$ is a source vector that characterizes the dipole strength distribution at radial location i, for the time harmonic s and circumferential harmonic q. Moreover,

$$H_{sjL} = -\frac{isk_1 \cos \vartheta_j}{2r_j} i^{sB+q} e^{isk_1 r_j} e^{i(sB+q)\varphi_j} \Delta r_1 J_{sB+q}(sk_1 r_{1i} \sin \vartheta_j) r_{1i}$$

is a transfer function relating the source strength f_{sL} to the radiated sound field p_{sj}. Eq. (13) is a linear system that can be brought in matrix form,

$$\mathbf{p}_s = \mathbf{H}_s \mathbf{f}_s, \tag{14}$$

where $\mathbf{p}_s$ is a vector of far-field acoustic pressures measured at J locations, $\mathbf{f}_s$ is a vector of coefficients for unsteady rotating axial forces per unit area exerted by the blades on the fluid and $\mathbf{H}_s$ is the transfer function between the force coefficients and the far-field acoustic pressure. All these quantities are defined for the multiple s of the BPF.

3.2. Formulation of the inverse model

The objective of the inverse model is to obtain the source vector $\mathbf{f}_s$ from measured far-field acoustic data $\mathbf{p}_s$. To achieve this, the problem can be transformed into the minimization of a quadratic function. We define the far-field acoustic pressure measurements $\hat{\mathbf{p}}_s$ to be equal to the predicted acoustic pressure plus an error $\mathbf{e}_s$

$$\hat{\mathbf{p}}_s = \mathbf{H}_s \mathbf{f}_s + \mathbf{e}_s. \tag{15}$$

The vector $\mathbf{f}_s$ can be obtained using the approach proposed by Nelson and Yoon [12] for the estimation of acoustic source strength by inverse methods. The cost function J_s to be minimized at $\omega = s\omega_1$ is defined as

$$J_s = \sum_{j=1}^{J} |e_{sj}|^2 = \mathbf{e}_s^H \mathbf{e}_s, \tag{16}$$

where H denotes the Hermitian transpose and e_{sj} is the error between the predicted and the measured acoustic pressure at the frequency $\omega = s\omega_1$ and location j. The minimization of J_s leads to the optimal estimate of the source force vector $\mathbf{f}_{s0}$

$$\mathbf{f}_{s0} = \mathbf{H}_s^+ \hat{\mathbf{p}}_s, \tag{17}$$

where $\mathbf{H}_s^+ = [\mathbf{H}_s^H \mathbf{H}_s]^{-1} \mathbf{H}_s^H$ designates the pseudo-inverse of the matrix $\mathbf{H}_s$. There is a single solution of this minimization provided $[\mathbf{H}_s^H \mathbf{H}_s]$ is positive definite. In our problem $\mathbf{f}_s^H [\mathbf{H}_s^H \mathbf{H}_s] \mathbf{f}_s = \mathbf{p}^H \mathbf{p}$ is positive, which implies that the minimum is unique. Moreover, if the number of measurement points J is equal to the number of terms $I(q_{max} - q_{min} + 1)$ of the source vector to be determined, the solution can be simply written $\mathbf{f}_{s0} = \mathbf{H}_s^{-1} \hat{\mathbf{p}}_s$. If $J < I(q_{max} - q_{min} + 1)$, the solution is not unique.

3.3. Conditioning the inverse model

The sensitivity of the solution ($\mathbf{f}_{s0}$) to small changes ($\delta\hat{\mathbf{p}}_s$) in $\hat{\mathbf{p}}_s$ is determined by the condition number κ of the matrix $\mathbf{H}_s$, which can be defined as

$$\kappa(\mathbf{H}_s) = \|\mathbf{H}_s\| \|\mathbf{H}_s\|^{-1} = \sigma_{max}/\sigma_{min}, \tag{18}$$

where $\|\mathbf{H}_s\|$ is the 2-norm of the matrix $\mathbf{H}_s$, and σ_{min} and σ_{max} are, respectively, the smallest and the largest singular value of $\mathbf{H}_s$. The sensitivity of the solution can be directly derived from this condition number [12]

$$\frac{\|\delta\mathbf{f}_{s0}\|}{\|\mathbf{f}_{s0}\|} = \kappa(\mathbf{H}_s) \frac{\|\delta\hat{\mathbf{p}}_s\|}{\|\hat{\mathbf{p}}_s\|}. \tag{19}$$

When κ is small, $\mathbf{H}_s$ is well conditioned and small deviations in the pressure vector do not produce significant changes $\delta\mathbf{f}_{s0}$ in the force vector solution. But when κ is large, the problem is said to be ill-posed because small changes in $\hat{\mathbf{p}}_s$ lead to considerably large errors in the solution. In order to avoid a large discrepancy in the singular values of $\mathbf{H}_s$ and therefore an ill-conditioned problem, a stabilization approach is used where the force term is multiplied by a penalty factor. This method leads to the following alternative cost function:

$$J_s = \mathbf{e}_s^H \mathbf{e}_s + \beta \mathbf{f}_s^H \mathbf{f}_s, \tag{20}$$

where β is a regularization factor. Finally, the solution of this new minimization problem is given by [12]

$$\mathbf{f}_{s0} = [\mathbf{H}_s^H \mathbf{H}_s + \beta\mathbf{I}]^{-1} \mathbf{H}_s^H \hat{\mathbf{p}}_s. \tag{21}$$
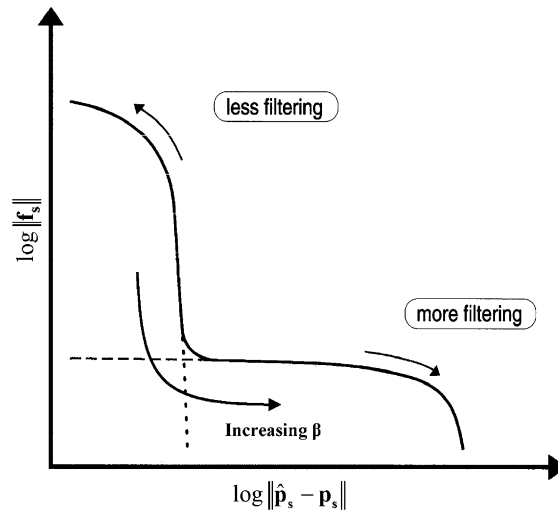
Fig. 2. The generic form of the L-curve. Adapted from Ref. [18] with the notations of the present paper.

3.4. Choice of the regularization parameter

The key point for a good regularization is a correct choice of the regularization parameter β. The approach used in this paper is the L-curve criterion [15,18]. The L-curve consists of plotting the 2-norm $\|\mathbf{f}_s\|$ of the regularized solution versus the residual 2-norm $\|\hat{\mathbf{p}}_s - \mathbf{p}_s\|$ in log–log scale, corresponding to various values of β. The generic L-curve is shown in Fig. 2 [18]. This curve can be decomposed into two regions: (1) in the part of the curve on the right of the corner, the solution is over-regularized, this situation is also called over-smoothing and (2) in the part of the L-curve above the corner, the regularized solution is dominated by the effects of error in the input data (such as measurement noise in the acoustic pressures $\hat{\mathbf{p}}_s$), the solution is under-regularized, this situation is called under-smoothing. In between these two regions, an optimal regularization parameter can be found, for which there is a trade-off between both under- and over-smoothing situations, such that the residual $\|\hat{\mathbf{p}}_s - \mathbf{p}_s\|$ is reasonably small and the regularized solution has a reasonably small norm $\|\mathbf{f}_s\|$ [15,18]. There are other methods to find the optimal regularization parameter but the L-curve criterion seems to be more robust [15,18] than the generalized cross-validation technique for example. In this paper, the optimal parameter corresponding to the maximum curvature of the L-curve corner is determined manually.

4. Numerical simulations

4.1. Sensitivity analysis

4.1.1. Setting

A typical automotive engine cooling fan is considered in the simulation, with the following parameters: exterior diameter $2a_2 = 30$ cm, interior diameter $2a_1 = 12.5$ cm, rotational speed

$\Omega/2\pi = 50\,\text{Hz}$ (the Mach number at blade tip is therefore 0.14), $B = 6$ blades with uniform blade pitch (the BPF is therefore 300 Hz). The fan radius is discretized into I equally spaced points r_{1i} ($1 \leqslant i \leqslant I$) in the interval $[a_1 a_2]$. The aeroacoustic sources over the fan area are defined according to Eq. (3), with $f_{sL} = \bar{f}_z^0(r_{1i})\alpha_s(r_{1i})\beta_q(r_{1i}) = 1$ when $q = -sB$ and $f_{sL} = \bar{f}_z^0(r_{1i})\alpha_s(r_{1i})\beta_q(r_{1i}) = 0$ when $q \neq -sB$. This simple situation corresponds to a sound radiation for a particular multiple of the BPF $\omega = s\omega_1$ due only to the circumferential harmonic $q = -sB$; in reality, the sound pressure at $\omega = s\omega_1$ as given by Eq. (8) is a combination of various circumferential harmonics q centred around $q = -sB$, but the circumferential harmonic $q = -sB$ has the largest contribution to the resulting sound pressure for subsonic fan operation. The far-field acoustic directivity was calculated according to Eq. (6) at J equally spaced downstream points, either on an arc of circle located in the (xz) plane ($\phi = 0$, Fig. 1), or on a hemispheric surface centred on the fan. The angles $\theta = -\pi/2$ and $+\pi/2$ (Fig. 1) were not included in the calculations of the far-field directivity since the zero acoustic pressure in these directions would render $\mathbf{H}$ singular.

The numerical scheme of the inverse model is: (1) impose unsteady aerodynamic forces $\mathbf{f}_s$ over the surface of the blade; (2) calculate the resulting acoustic pressure at the far-field points according to Eq. (14) (direct model); (3) reconstruct the forces $\mathbf{f}_{s0}$ using Eq. (21) (inverse model). The results of the direct model are plotted in Fig. 3 in terms of the dipole strength distribution and downstream acoustic directivity at the BPF ($s = 1$). Note that the acoustic directivity of the fan has been superposed with the acoustic directivity of a monopole of identical on-axis directivity. These results show that only the circumferential harmonic $q = 6$ of the dipole strength in Eq. (2) contributes to the far-field sound; moreover, the acoustic directivity of the fan in this case is perfectly dipolar.

In order to account for the presence of noise in the inverse model, a random noise is added to the "measured" far-field data as follows:

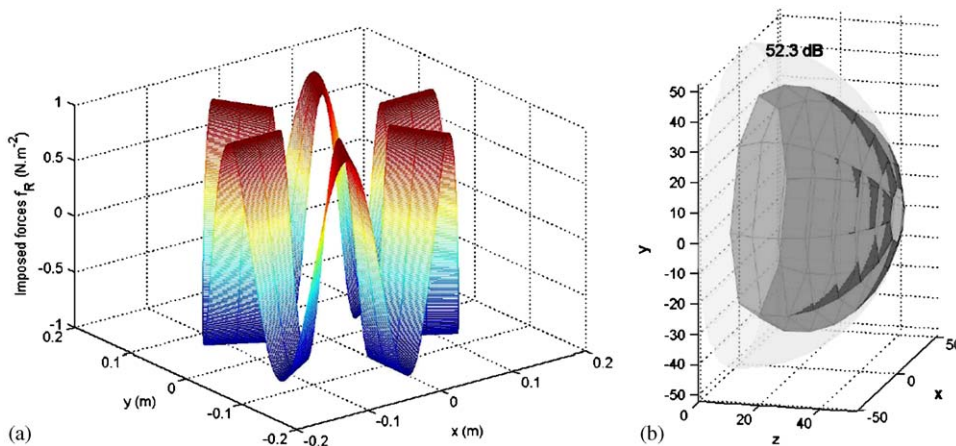$$\mathbf{p}_{sn} = \mathbf{p}_s + \mathbf{e}_n,$$

Fig. 3. Numerical results of the direct model at the BPF ($s = 1$), $2a_2 = 30\,\text{cm}$, $2a_1 = 12.5\,\text{cm}$, $\Omega/2\pi = 50\,\text{Hz}$, $B = 6$; (a) imposed dipole strength distribution; (b) far-field acoustic directivity. The acoustic directivity of the fan has been superimposed with the acoustic directivity of a monopole of identical on-axis directivity (pale grey surface).

where $\mathbf{p}_s$ is the prediction from the direct model, Eq. (14), $\mathbf{p}_{sn}$ is a noisy prediction and $\mathbf{e}_{sn}$ is a normally distributed random error vector which has a zero mean and a variance σ^2. The signal-to-noise (S/N) ratio is defined as

$$\frac{S}{N} = 20 \log_{10} \left[\frac{1}{J} \frac{|\mathbf{p}_s|^2}{\sigma^2} \right]^{1/2}. \tag{22}$$

In the following sections, the inverse model is analysed in terms of the regularization parameter β, the geometrical sensor arrangement, the frequency and the S/N ratio. Moreover, the spatial discretization of the fan used in the source reconstruction assumes $I = 3$ equally spaced points r_{1i} ($1 \leqslant i \leqslant 3$) in the radial direction and 9 circumferential harmonics of the dipole strength distribution ($q_{\min} = -sB - 4$, $q_{\max} = -sB + 4$). Therefore the dimension of the unknown source vector $\mathbf{f}_s$ is $I(q_{\max} - q_{\min} + 1) = 27$.

4.1.2. Influence of the regularization parameter β

The inverse model is ill-posed, which means that small errors in the input data lead to large perturbations in the solution if no care is taken in the choice of β. The case of a zero noise ($S/N = \infty$), $s = 1$ (aeroacoustic sources at the BPF) and $J = 64$ downstream far-field points regularly spaced on a hemispheric surface is first chosen in order to study the influence of β on the reconstructed unsteady force and the reconstructed acoustic directivity. In this case, the condition number κ of the matrix $\mathbf{H}_s$ is large (7×10^{10}), which means that the problem is ill-conditioned.

Fig. 4 shows the reconstructed dipole strength distribution over the fan area and the reconstructed downstream far-field directivity for various values of β. These results are to be compared to the imposed data of Fig. 3. When no regularization of the inverse problem is imposed ($\beta = 0$), contributions of other circumferential Fourier modes than $q = -sB$ lead to errors in the magnitude of the reconstructed force and the reconstructed and imposed acoustic radiation neither fit in magnitude nor in directivity. For large values of β (10^0), the distribution of the reconstructed force is correct but the magnitude is much smaller than the imposed one, because such large values of β significantly decrease the ratio between the smallest and the largest singular value of $\mathbf{H}_s$; moreover, the estimated acoustic radiation is erroneous in this case. The intermediate value $\beta = 10^{-10}$ yields a satisfactory reconstruction of both the aeroacoustic sources and acoustic far-field.

Fig. 5 shows the L-curves associated to the inversion of the system at BPF and its first three harmonics. As already noted by several authors [11,12,15], the regularization parameter is not an arbitrary choice. In the case depicted here, the values $10^{-12} < \beta < 5 \times 10^{-4}$ provides an optimal reconstruction range for which $\|\mathbf{f}_s\|$ is constant as a function of β and leads to a good match between the estimated acoustic pressure and the imposed acoustic field. As demonstrated in Ref. [18], for a very small β, the L-curves do not have a vertical branch in the uppermost part but a horizontal asymptote since no noise is added to the input acoustic pressure vector.

4.1.3. Influence of the S/N ratio

A random noise (normal distribution with zero average) is now algebraically added to the imposed far-field data as given by Eq. (22). The influence of S/N on the reconstruction is analysed in terms of the inversion of the system at BPF via the L-curve behaviour in Fig. 6. When measurement noise is added, a vertical asymptote appears for low values of the regularization
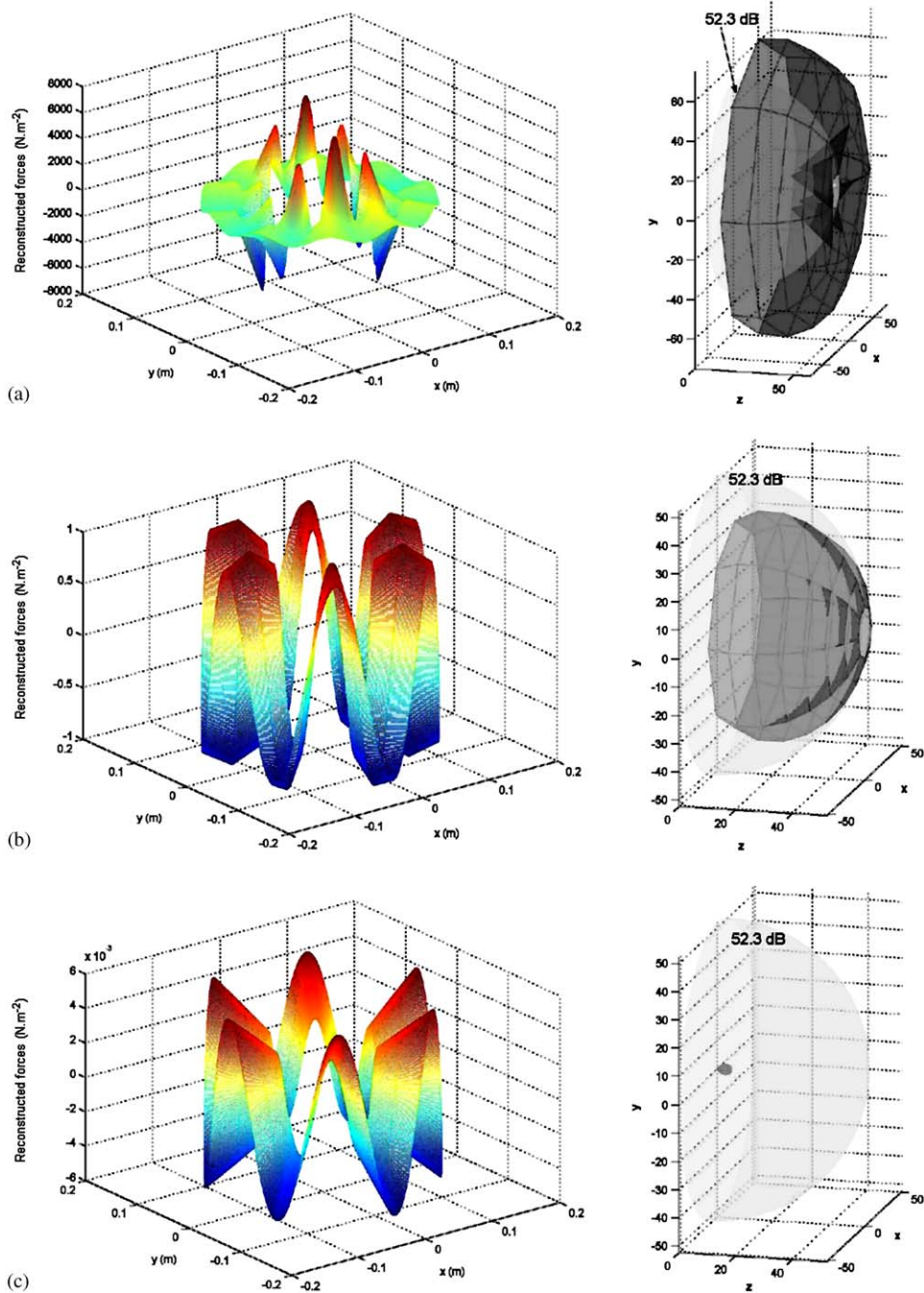
Fig. 4. Left-hand column: reconstructed dipole strength distribution over the fan area at 1 BPF ($s = 1$) and right-hand column: reconstructed downstream far-field directivity for various values of the regularization parameter β: (a) $\beta = 0$, (b) $\beta = 10^{-10}$, (c) $\beta = 10^{-0}$. Zero noise ($S/N = \infty$), $J = 64$ far-field points on a downstream hemispheric surface. The acoustic directivity of the fan has been superimposed with the acoustic directivity of a monopole of identical on-axis directivity (pale grey surface).
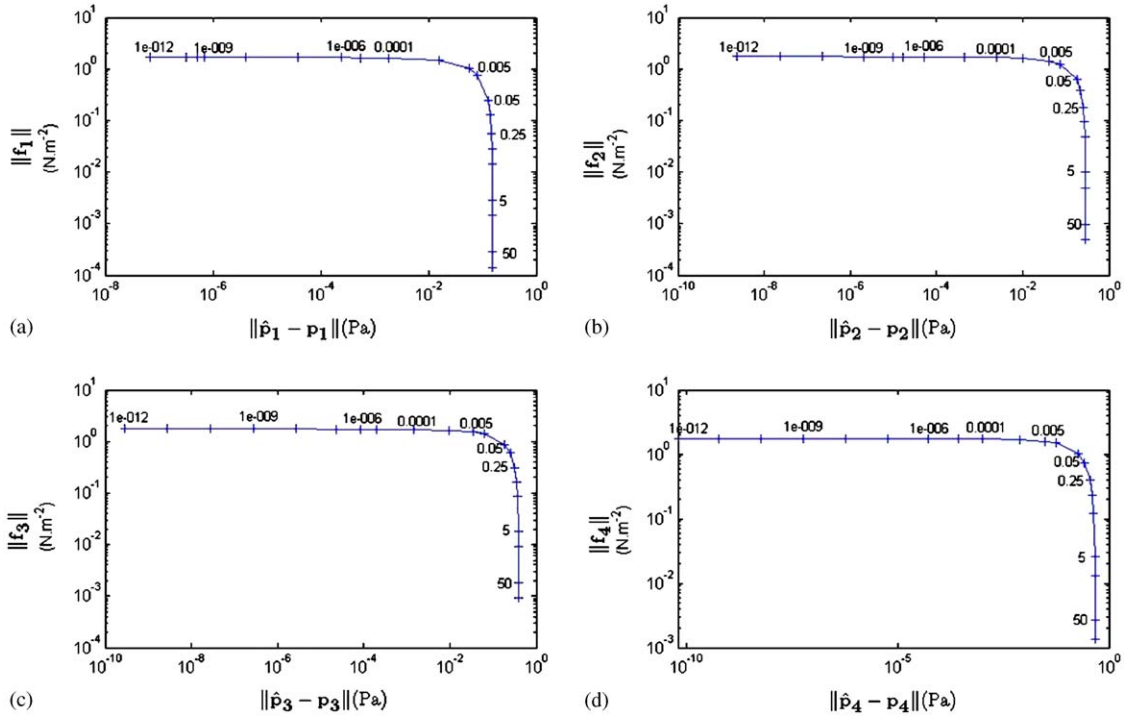
Fig. 5. L-curves corresponding to the source reconstruction at BPF and its first three harmonics. (a) $s = 1$, (b) $s = 2$, (c) $s = 3$, (d) $s = 4$. Zero noise ($S/N = \infty$), $J = 64$ far-field points on a downstream hemispheric surface. The values of β are indicated on the curves.

parameter. Moreover, Fig. 6 shows that the region of optimal reconstruction with respect to the regularization parameter narrows as S/N increases. The optimal values of β corresponding to the L-curve corners are about 10^{-6}, 10^{-5} and 10^{-3} for the S/N ratios of 20, 5 and 1 dB, respectively, which means that more filtering is required when adding noise in the input data. A satisfactory reconstruction of the far-field data not leading to excessive values of the forces $\|\mathbf{f}_s\|$ is achievable for a S/N ratio up to 0 dB.

4.1.4. Influence of the geometrical arrangement of sensors

The inverse problem is now investigated with respect to the geometrical arrangement of downstream far-field acoustic sensors. Two arrangements are investigated (Fig. 7): a circular arc located in the plane $\varphi = 0°$ and extending from $\vartheta = -80°$ to $80°$, or a regular distribution on a hemispheric surface. In both cases, 64 sensors are assumed. Fig. 8 shows the condition number $\kappa(\mathbf{H})$ as a function of frequency for the two sensor arrangements and for $s = 1$, $I = 3$. At low frequency, the condition number κ is large for both sensor arrangements; the resulting poor conditioning of the inverse problem is due to the insufficient spatial resolution of the source for frequency below 200 Hz. As the frequency increases, the condition number improves for the hemispheric arrangement of sensor while κ remains large for the circular arrangement. As expected, a circular sensor arrangement is therefore less appropriate than a hemispheric arrangement to reconstruct the surface source distribution.
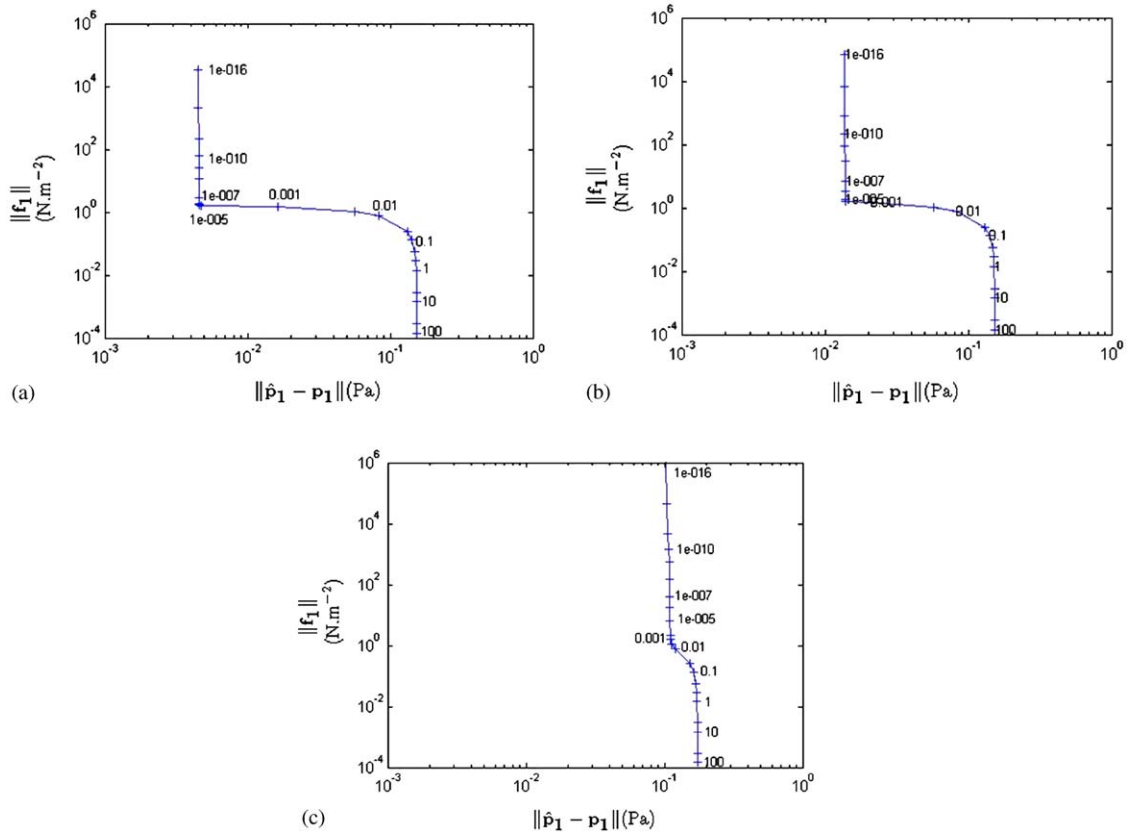
Fig. 6. L-curves corresponding to the inversion of BPF for various values of the signal-to-noise ratio S/N: (a) $S/N = 20\,\mathrm{dB}$, (b) $S/N = 5\,\mathrm{dB}$, (c) $S/N = 1\,\mathrm{dB}$. $J = 64$ far-field points on a downstream hemispheric surface. The values of β are indicated on the curves.

In order to test the ability of the circular sensor arrangement to reconstruct the forces $\mathbf{f}_s$, the source reconstruction is conducted with $\Omega/2\pi = 50\,\mathrm{Hz}$, $\beta = 10^{-5}$, $s = 1$, $S/N = 20\,\mathrm{dB}$. The optimal reconstruction (Fig. 9) shows that the inverse model is able to reconstruct the forces from 64 measurement points located on a circular arc even if the transfer matrix $\mathbf{H}$ is badly conditioned. From these estimated forces, a correct acoustic directivity is reconstructed. This can be explained by the dipole axial symmetry radiated by the imposed forces described in the setting.

4.2. Simulation of fan source reconstruction for non-uniform flow

To illustrate the inverse model for non-uniform flow condition, the following case is considered: the source strength function $f_z^0(r_1, \varphi_1)$ of Eq. (2) is given by

$$f_z^0(r_1, \varphi_1) = \begin{cases} 1 & \text{if } -\dfrac{\Phi_1}{2} + 2n\pi \leqslant \varphi_1 \leqslant +\dfrac{\Phi_1}{2} + 2n\pi, \\ 0 & \text{otherwise.} \end{cases} \tag{23}$$
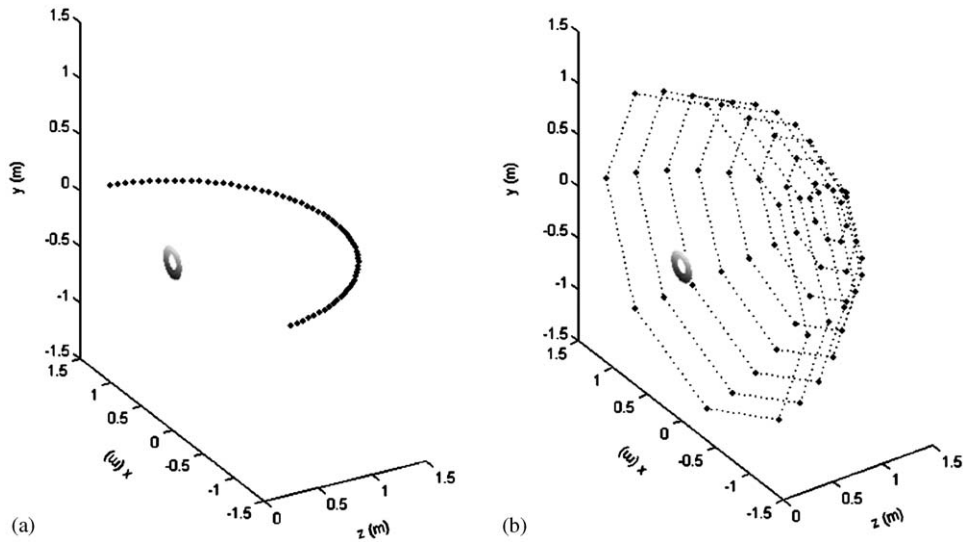
Fig. 7. Downstream radiation space meshing (the radiation surface of the fan is shown at the centre). (a) 64 sensors on an arc of a circle from $\vartheta = -80°$ to $80°$ and $\varphi = 0°$, and (b) 64 sensors on a hemispheric surface.
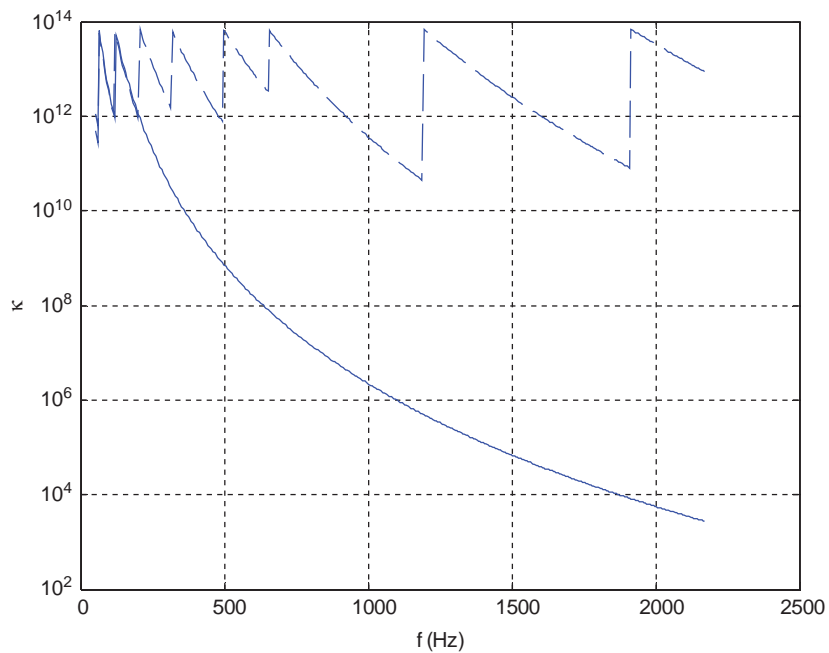

Fig. 8. Condition number κ of the matrix $\mathbf{H}$ as a function of f for different sensor arrangements. $I = 3$, $s = 1$, $q_{min} = sB - 4$, $q_{max} = sB + 4$. $J = 64$ measurements points (solid: on a hemispheric surface, dashed: on an arc of a circle as shown in Fig. 7).
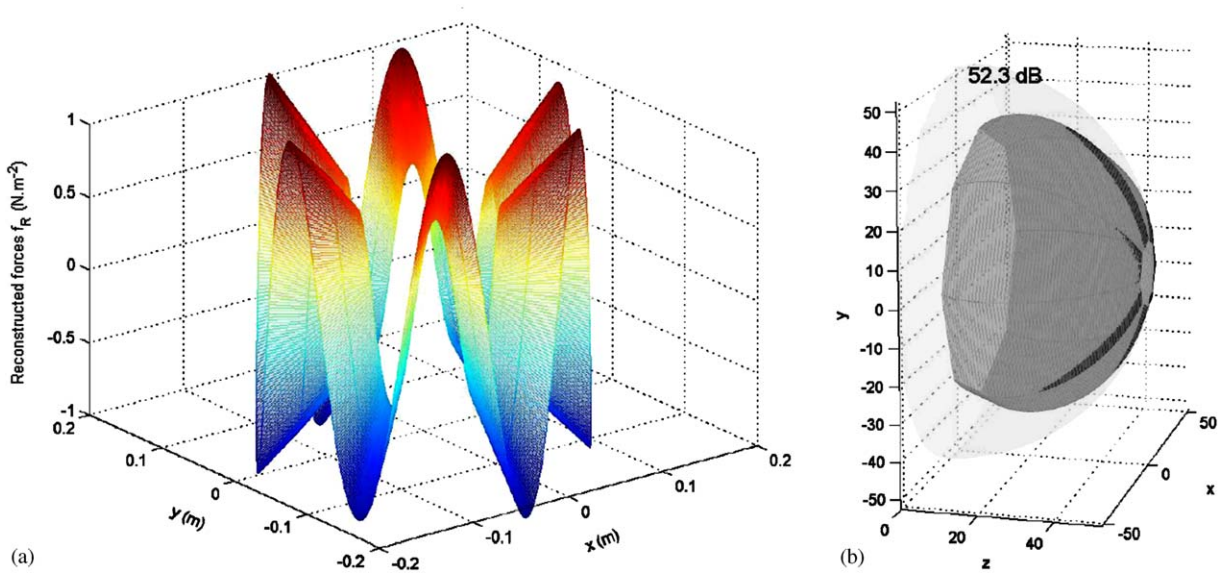
Fig. 9. (a) Reconstructed dipole strength distribution over the fan area and (b) reconstructed downstream far-field directivity for $\beta = 10^{-5}$, $s = 1$, $S/N = 20$ dB. $J = 64$ far-field points on arc of a circle. The acoustic directivity of the fan has been superimposed with the acoustic directivity of a monopole of identical on-axis directivity (pale grey surface).

This situation describes a spatial variation of the source distribution in the circumferential direction, and may therefore represent a strongly circumferentially non-uniform flow. From Eq. (2), the circumferential Fourier coefficients β_q are given in this case by

$$\beta_q(r_1) = \frac{\Phi_1}{2\pi} \frac{\sin(q\Phi_1/2)}{q\Phi_1/2}.$$

Moreover, the circumferential average $\bar{f}_z^0(r_1)$ and the time Fourier coefficients $\alpha_s(r_1)$ are arbitrarily set to unity and Φ_1 is set to $15°$. Therefore, the coefficients of the imposed unsteady rotating force vector $\mathbf{f}_s$ in Eq. (14) reduce to $f_{sL} = \bar{f}_z^0(r_{1i})\alpha_s(r_{1i})\beta_q(r_{1i}) = \beta_q$. All other data are similar to the previous sections ($B = 6$, $\Omega/2\pi = 50$ Hz). Fig. 10 shows the corresponding dipole strength distribution over the fan area and its circumferential Fourier series decomposition (truncated to order 60) along 2 radii: $r_1 = 8$ and 14 cm.

In this example, the inversion is carried out for the first 4 harmonics of the BPF ($s = 1, 2, 3, 4$), the propeller was discretized in 2 circles ($I = 2$) located at $r_{11} = 8$ cm and $r_{12} = 14$ cm and the number of circumferential harmonics q is chosen such that $q_{min} = -sB - 2$, $q_{max} = -sB + 3$, thus $Q = 6$; the dimension of the unknown source vector $\mathbf{f}_s$ is therefore $I(q_{max} - q_{min} + 1) = 12$. Finally, $J = 36$ acoustic pressure sensors are simulated on a hemispheric surface 1.5 m downstream the fan, with a S/N ratio of 5 dB.

The condition number of the transfer matrix $\mathbf{H}$ is given by $\kappa = 3.7 \times 10^4$ at BPF ($s = 1$), $\kappa = 2.1 \times 10^3$ at 2 BPF ($s = 2$), $\kappa = 380$ at 3 BPF ($s = 3$), and $\kappa = 108$ at 4 BPF ($s = 4$). Optimal values of the regularization parameter derived from the corresponding L-curve corners
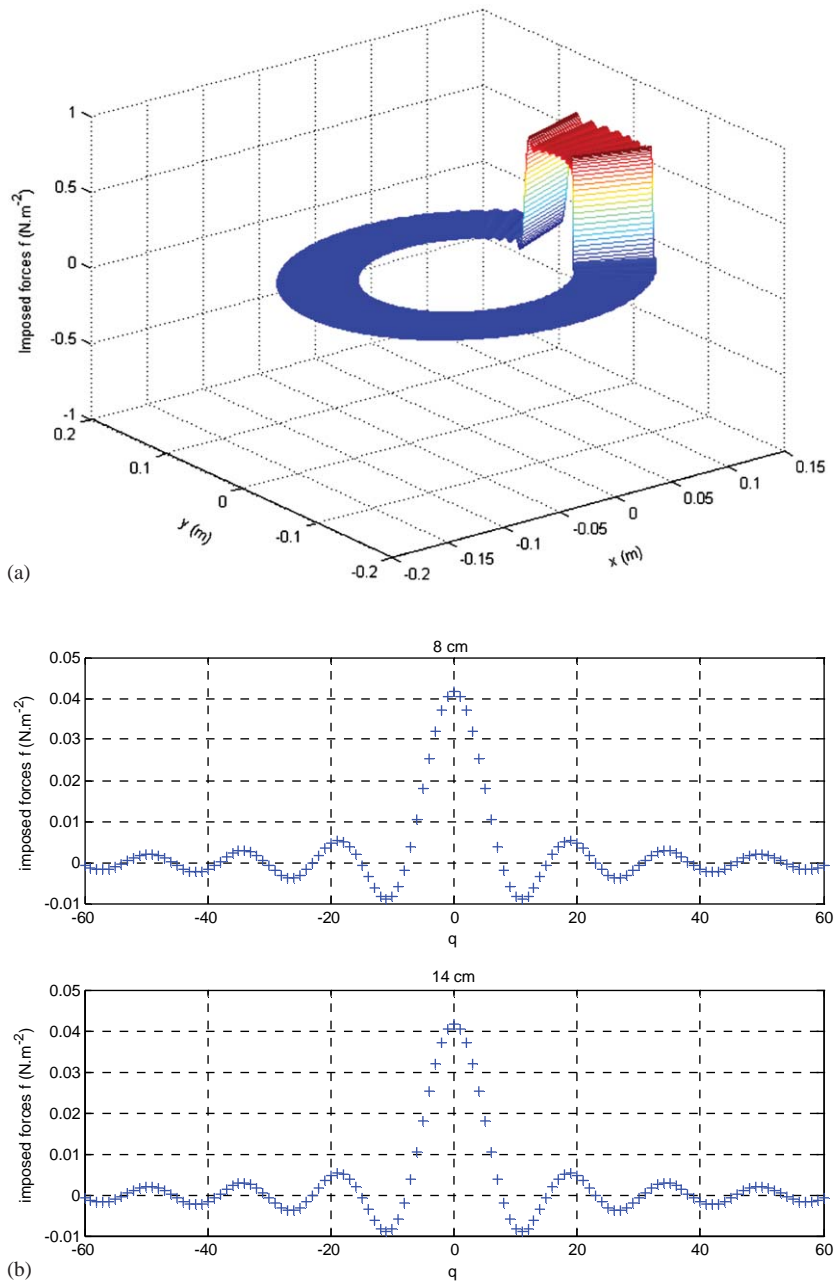
Fig. 10. (a) Imposed dipole strength distribution over the fan area and (b) its circumferential Fourier series decomposition (truncated to order 60) along 2 radii: $r_1 = 8$ cm and $r_1 = 14$ cm (right).

are: $\beta = 5 \times 10^{-7}$ for $s = 1$ and $\beta = 10^{-4}$ for $s = 2, 3, 4$. These values were found to be sufficient to provide both accurate reconstruction of the far-field data and acceptable values of the force per unit area vector $\|\mathbf{f}_s\|$.

This section focuses on the ability of the inverse model to reconstruct the dipole strength distribution of Fig. 10, both in the spatial and circumferential wavenumber domains. Fig. 11 presents the results of the inverse model for the first four harmonics of BPF $s = 1, 2, 3, 4$. These results show that the circumferential location of the maximum force acting by the blade on the fluid can be predicted from the inversion at each of the 4 harmonics, but the imposed distribution of Fig. 10 cannot be accurately reconstructed from each of these those plots. Moreover, the circumferential wavenumber spectrum of the reconstructed force distribution is generally in good agreement with the imposed force spectrum, especially for the outer radial element (low order circumferential harmonics are poorly reconstructed at the inner radial element for $s = 1$). Finally, the source distributions for the first four harmonics of BPF $s = 1, 2, 3, 4$ are superposed in Fig. 12 to represent the complete circumferential wavenumber spectrum of the unsteady forces. The superposition of the forces estimated from the first four harmonics significantly improves the quality of the reconstruction. The reconstructed force distribution is close to the imposed
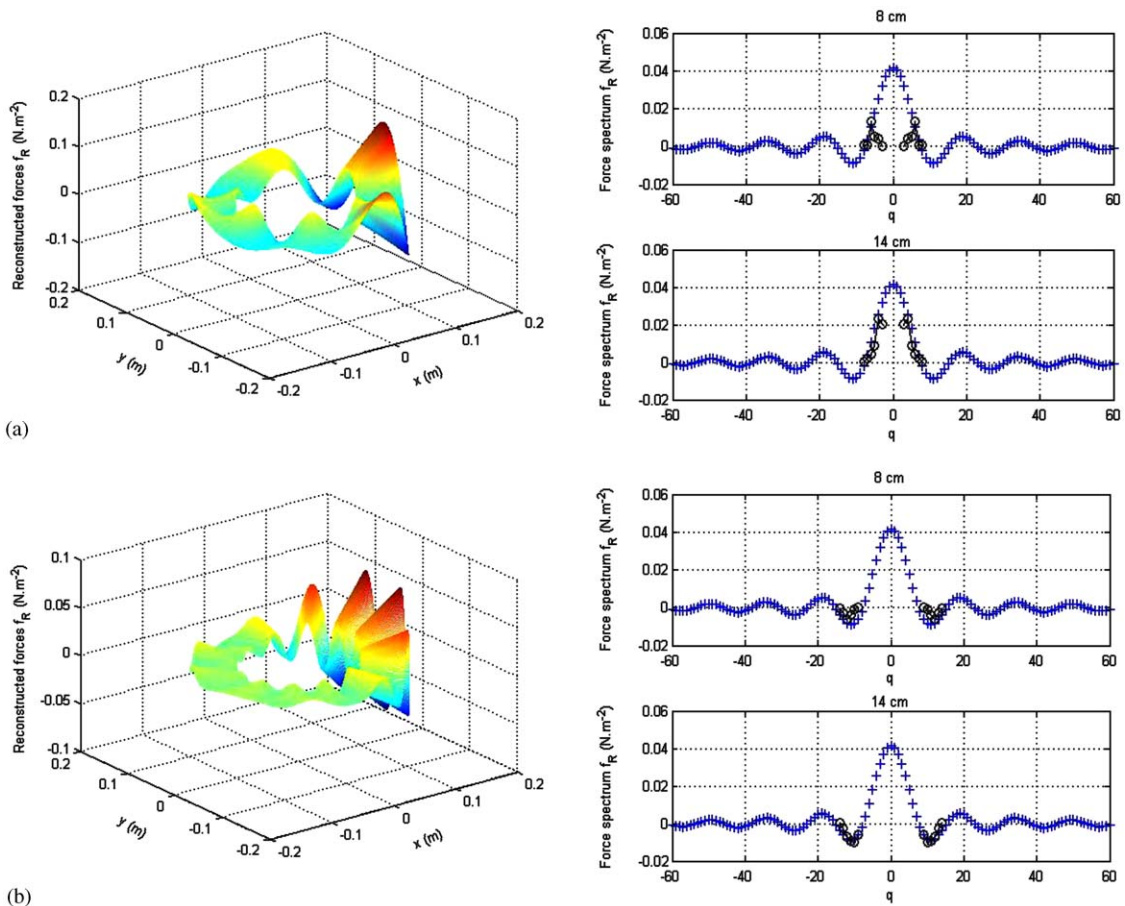

Fig. 11. Left-hand column: reconstructed dipole strength distribution over the fan area, and right-hand side column: its circumferential Fourier series decomposition (truncated to order 60) along 2 radii: $r_1 = 8$ cm and $r_1 = 14$ cm. (a) $s = 1$, (b) $s = 2$, (c) $s = 3$, (d) $s = 4$. $S/N = 5$ dB, $J = 36$ far-field points on a downstream hemispheric surface.
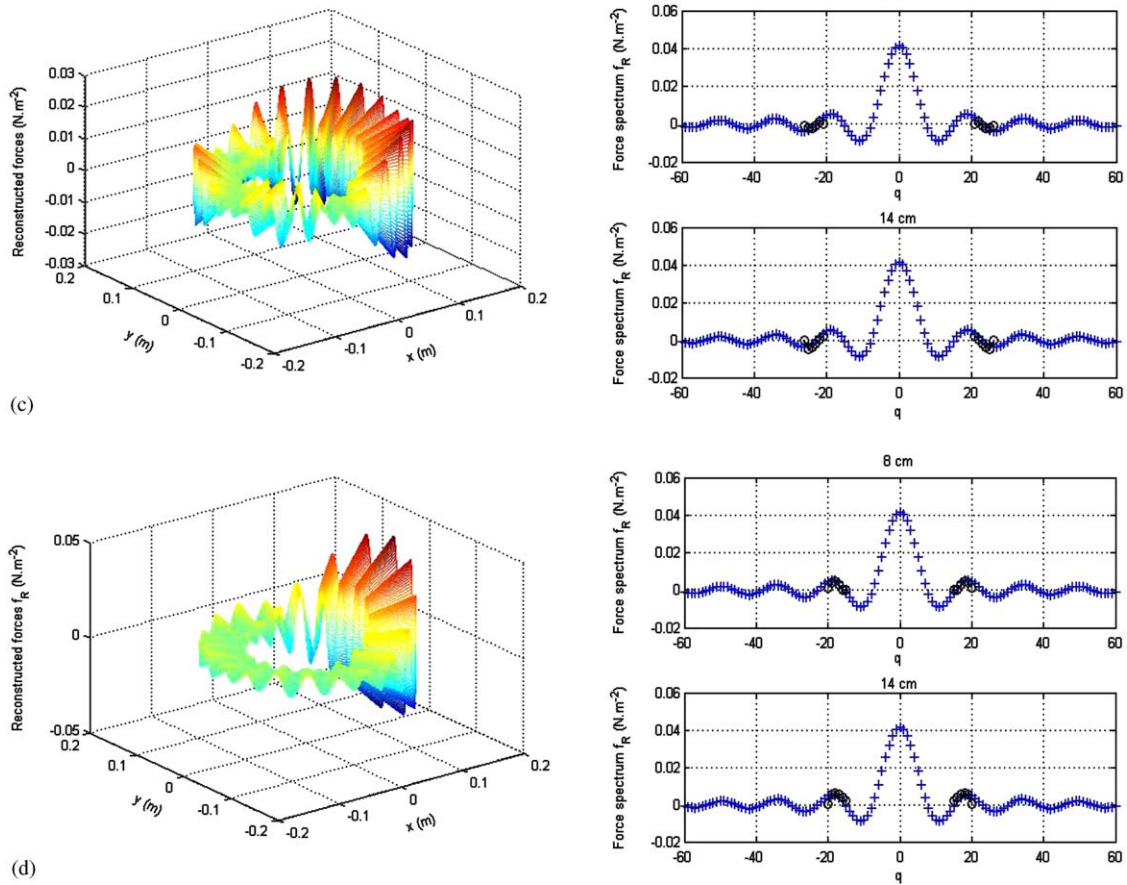
Fig. 11. (*Continued*)

distribution of Fig. 10; however, the magnitude of the reconstructed forces is not as large as the amplitude of the imposed forces because low order circumferential harmonics are not properly reconstructed over the whole radiation surface.

To summarize, the inverse model is able to partially reconstruct the unsteady rotating forces acting by the blades on the fluid and thus locate "hot spot" non-uniform flow entering the fan. The acoustic signature of the fan measured at a relatively low number of locations is a useful tool to derive the unsteady behaviour of the fluid near the propeller surface even in presence of measurement noise.

5. Preliminary experimental results

5.1. Experimental set-up

The inversion procedure to extract aeroacoustic source distributions from far-field acoustic data was tested on an automotive axial fan. Experiments were conducted on an engine cooling
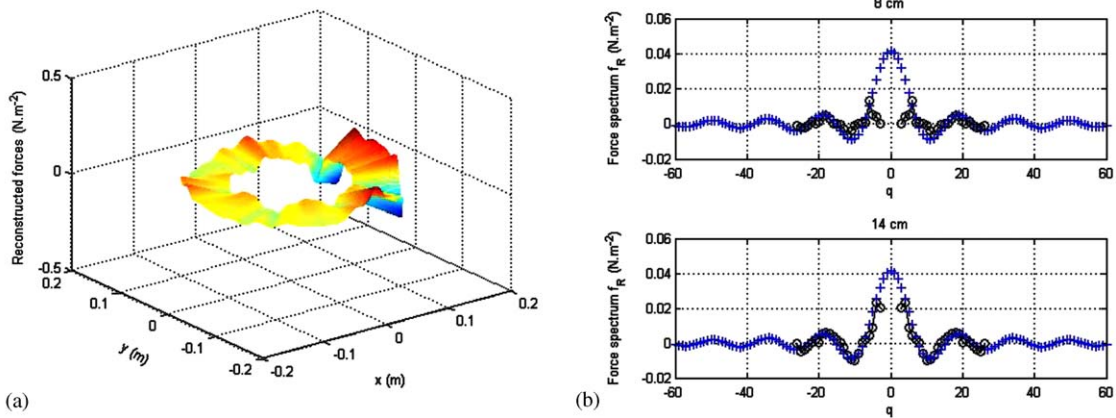
Fig. 12. Representation of the axial forces acting by the rotor on the fluid per unit surface: (a) reconstructed forces in the plane of the fan and (b) circumferential Fourier series decomposition (bilateral spectrum), up: inner radius 8 cm; down: outer radius 14 cm; $+$, imposed forces; $\circ$, reconstructed forces. $S/N = 5\,\text{dB}$, $V = 2$, $Q_1 = -sB - 2$, $Q_2 = -sB + 3$, $s = 1, 2, 3, 4$; $J = 36$ on a hemispheric surface.

unit consisting of a symmetric six-bladed ($B = 6$) axial fan and a radiator. The fan has an exterior diameter of 30 cm and a central hub of 12.5 cm in diameter. A small ($4 \times 8\,\text{cm}^2$) rectangular piece of adhesive tape was bonded on the upstream side of the radiator at about 5 cm from the fan axis in order to enhance the non-uniformity of the incoming flow and therefore increase tonal noise radiation. The unit was driven by a variable DC source (0–20 V/0–60 A) which was adjusted to set a rotational speed of the fan of 50 Hz. The set-up was placed in a semi-anechoic room with the fan axis horizontal and at 50 cm above the ground, and absorbing material was placed on the ground under the set-up in order to minimize ground reflections (Fig. 13).

For simplicity, acoustic measurements were performed at $J = 17$ equally spaced locations on a arc of a circle in the horizontal plane at 1.5 m from the fan centre. The microphone directions ranged from $\theta = -80°$ to $80°$ from the fan axis. A circular arrangement of sensors was found sufficient to provide a satisfactory source reconstruction in theory when the radiated sound field is axi-symmetric (Fig. 9). This is especially true at BPF, where the measured radiated sound field is almost dipolar and the circumferential harmonic of the force $q = 6$ is found to be the main contributor. The circular arrangement is still expected to provide an acceptable solution for the first harmonic of the BPF, where the experimental directivity showed a dipolar radiation slightly shifted from the fan axis. A windscreen was mounted on the microphone to minimize the effect of flow noise. Far-field conditions from the fan centre are found at distances over 1.5 m since this distance is much larger than the propeller radius and represents approximately 1.3 wavelengths for $s = 1$ (300 Hz) and 2.6 wavelengths for $s = 2$ (600 Hz). Note that the measured quantity was the far-field *acoustic power spectrum* (obtained by averaging 20 time sequences for a given location) using a single microphone which was sequentially moved over the arc of a circle, in order to further remove flow noise from the acoustic data. Therefore, the phase variations of the acoustic pressure over the circular arc were not considered in the source reconstruction scheme.

In the inversion scheme, the propeller was discretized in 2 circles ($I = 2$) located at $r_{11} = 8\,\text{cm}$ and $r_{12} = 14\,\text{cm}$ and the number of circumferential harmonics q is chosen such that
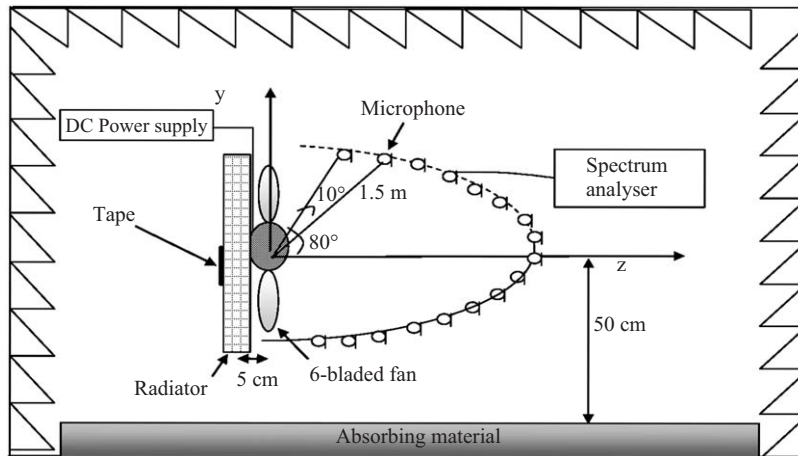
Fig. 13. Experimental set-up.

$q_{\min} = -sB - 3$, $q_{\max} = -sB + 3$ $Q = 7$; therefore the dimension of the unknown source vector $\mathbf{f}_s$ is $I(q_{\max} - q_{\min} + 1) = 14$. The condition number in this case is $\kappa = 8.9 \times 10^8$ at BPF ($s = 1$) and $\kappa = 6.5 \times 10^5$ at 2 BPF ($s = 2$). The inversion problem for such a configuration is relatively ill-conditioned because the acoustic sensors cover only an arc of a circle instead of the whole downstream half-space (see Section 4.1).

5.2. Experimental results

Figs. 14 and 15 show the reconstructed dipole strength distribution over the fan area and the measured and reconstructed far-field directivity over the sensor arc at BPF and at 2 BPF, for various values of the regularization parameter. Fig. 16 shows the corresponding L-curves for $s = 1$ and 2.

A value of $\beta = 10^{-6}$ corresponding to the corner of the two L-curves of Fig. 16 was chosen for the regularization parameter for both $s = 1$ and 2 since it provides a reasonably small error $\|\hat{\mathbf{p}}_s - \mathbf{p}_s\|$ without leading to an excessive value of the source strength $\|\mathbf{f}_s\|$. The measured and estimated directivity at $s = 1$ (Fig. 14) and $s = 2$ (Fig. 15) are in good agreement for $\beta = 10^{-6}$. The measured and reconstructed directivity at $s = 1$ is axi-symmetric and dipolar. As expected, the dipole strength distribution over the fan shows a dominant $q = SB = 6$ circumferential harmonic for $\beta = 10^{-6}$. However, the measured and reconstructed directivity at $s = 2$ is not symmetric with respect to the fan axis. In this case, a superposition of several circumferential harmonics is necessary to reproduce the measured acoustic directivity for $\beta = 10^{-6}$. It can be noticed however that the value of the estimated source strength is rather sensitive to the value of the regularization parameter. This large sensitivity results from the poor conditioning of the problem when simply a circular arrangement of sensor is used to reconstruct a source strength distribution over the source area. Grace et al. [11] made similar observations in the context of a slightly different inverse model.
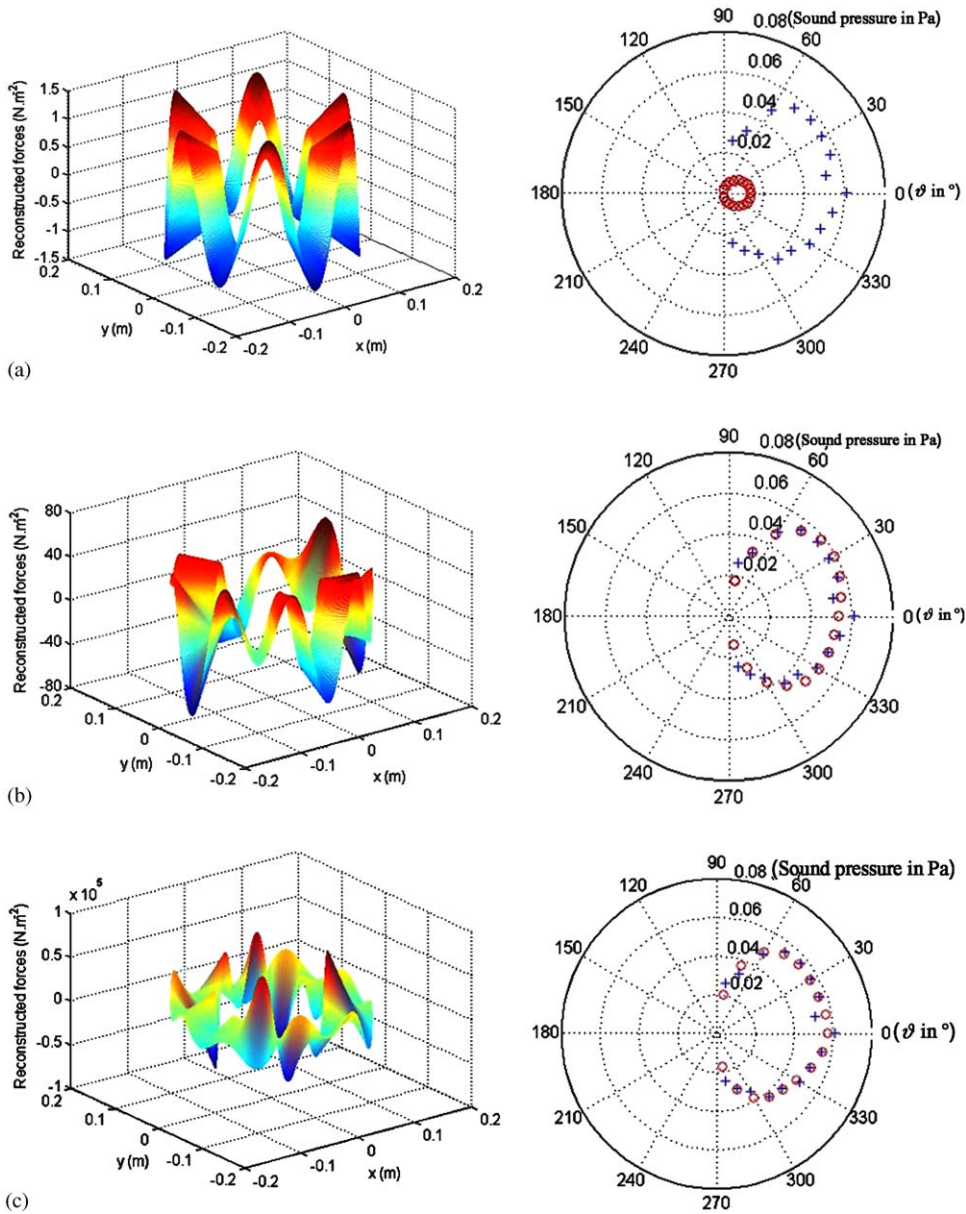
Fig. 14. Left-hand column: reconstructed dipole strength distribution over the fan area at 1 BPF ($s = 1$) and right-hand column: reconstructed far-field directivity ($+$, measured directivities; $\circ$, reconstructed directivities) for various values of the regularization parameter β: (a) $\beta = 10^{-2}$, (b) $\beta = 10^{-6}$, (c) $\beta = 10^{-14}$. $J = 17$ *measured* points on a downstream arc of a circle.

6. Conclusion

An inverse aeroacoustic model aiming at reconstructing the aerodynamic forces (dipole strength distribution) acting by the fan blades at multiples of the BPF on the fluid has been
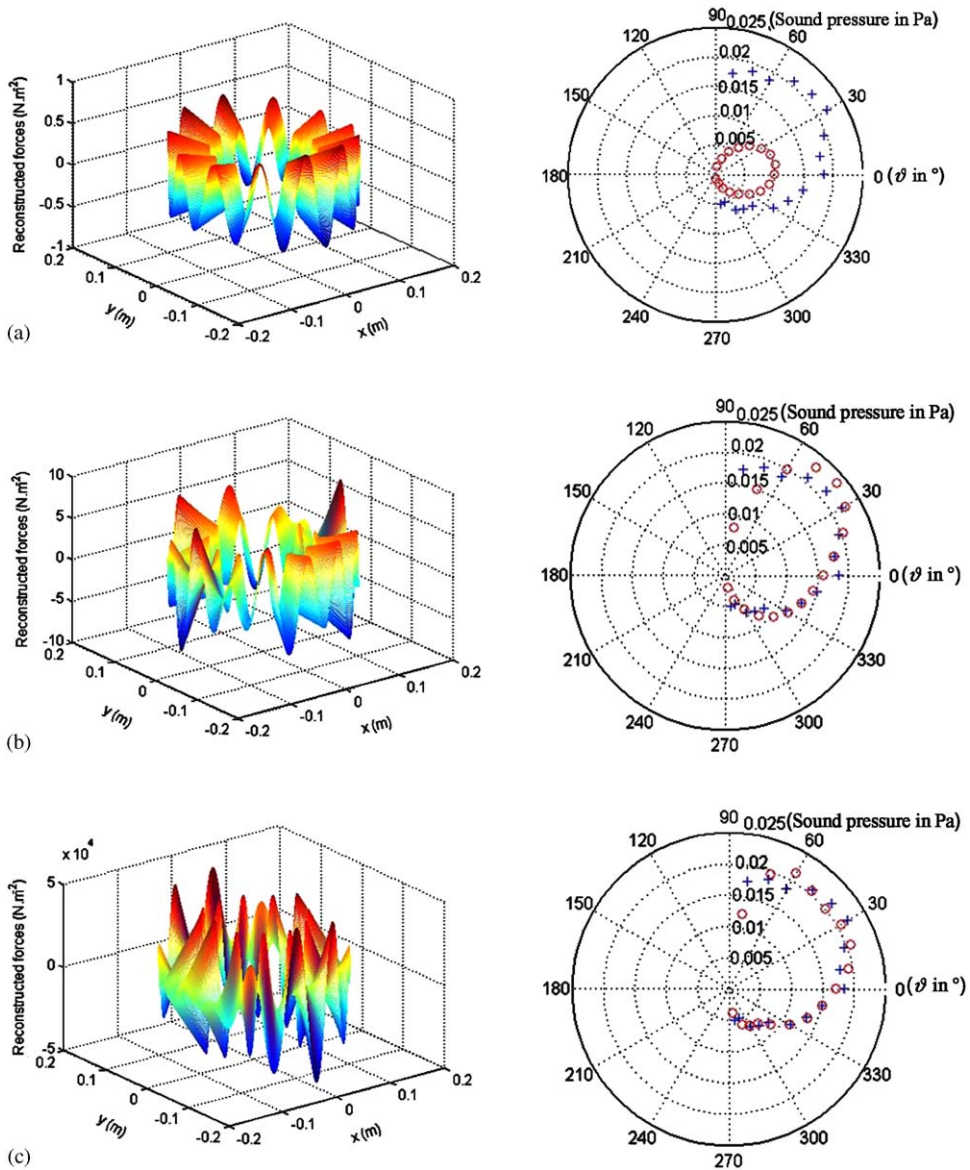
Fig. 15. Left-hand column: reconstructed dipole strength distribution over the fan area at 2 BPF ($s = 2$), and right-hand column: reconstructed far-field directivity ($+$, measured directivities, $\circ$, reconstructed directivities) for various values of the regularization parameter β: (a) $\beta = 10^{-2}$, (b) $\beta = 10^{-6}$, (c) $\beta = 10^{-14}$. $J = 17$ *measured* points on a downstream arc of a circle.

developed. It is based on a discrete form of Morse and Ingard's analytical direct model that relates the unsteady forces to the radiated sound field. To overcome the ill-conditioning of the inverse problem, a penalization of the source strength is used to stabilize the solution. Numerical
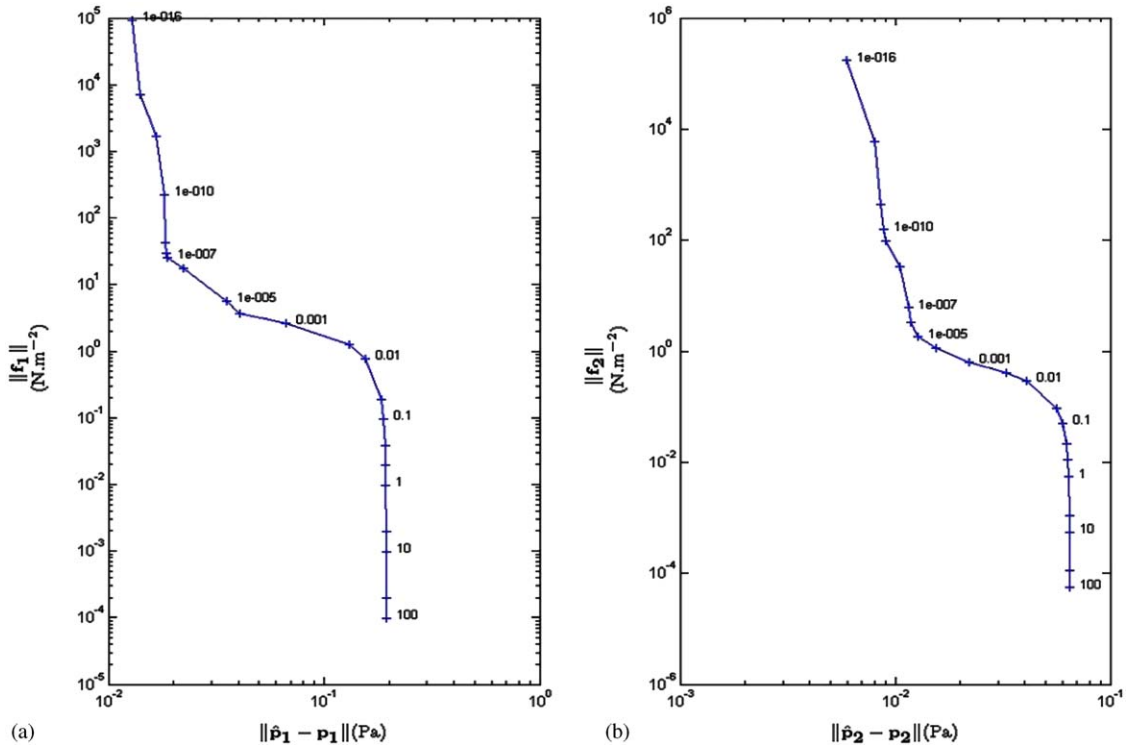
Fig. 16. L-curves corresponding to the source reconstruction at: (a) BPF ($s = 1$), and (b) 2BPF ($s = 2$). $J = 17$ measured points on a downstream arc of circle. The values of β are indicated on the curves.

simulations and experimental results for an engine cooling fan demonstrate the ability of the inverse model to reconstruct the dipole strength distribution over the fan surface, and possibly locate acoustic "hot spots" of the fan resulting from circumferentially non-uniform upstream flow, under realistic conditions of S/N ratio and acoustic far-field sensing arrangement. This method can thus serve as a non-intrusive technique to estimate the unsteady forces acting on the rotating blades and a tool for studying the interaction between a non-uniform flow and a rotor. In the second part of this paper, the inverse model is exploited in order to derive optimal control source and error sensor arrangements for active control of tonal noise from engine cooling axial fans.

Acknowledgments

References

[1] J.E. Ffowcs Williams, D.L. Hawkings, Sound generated by turbulence and surfaces in arbitrary motion, *Philosophical Transactions of the Royal Society of London* A 264 (1969) 321–342.

[2] S.E. Wright, Sound radiation from a lifting rotor generated by asymmetric disk loading, *Journal of Sound and Vibration* 9 (2) (1969) 223–240.

[3] M.V. Lowson, Theoretical analysis of compressor noise, *Journal of the Acoustical Society of America* 47 (1 (Part 2)) (1968) 371–385.

[4] P.M. Morse, K.U. Ingard, *Theoretical Acoustics*, Princeton University Press, Princeton NJ, 1986 925p.

[5] M.E. Goldstein, *Aeroacoustics*, McGraw-Hill International, New York, 1976 293p.

[6] W.H. Jeon, Overview of numerical analysis of fan noise, *Proceedings of Fan Noise 2003*, Senlis, France, 2003.

[7] C. Raffaitin, M. Roger, L. Rufer, M. Fabicki, Caractérisation des sources de bruit aérodynamique sur un ventilateur centrifuge à flux axial, *Journal de Physique* C5 (4) (1994) 985–988.

[8] M. Staiger, H. Stetter, Periodic response of axial fan rotor blades to nonuniform inlet flow fields, *International Gas Turbine and Aeroengine Congress and Exhibition*, Birmingham, UK, 1996.

[9] X.D. Li, S. Zhou, Spatial transformation of the discrete sound field from a propeller, *AIAA Journal* 34 (6) (1996) 1097–1102.

[10] J. Luo, X.D. Li, An inverse aeroacoustic problem on rotor wake/stator interaction, *Journal of Sound and Vibration* 254 (2002) 219–229.

[11] S.P. Grace, H.M. Atassi, Inverse aeroacoustic problem for a streamlined body—Part 1: basic formulation, Part 2: accuracy of solutions, *AIAA Journal* 34 (1996) 2233–2240.

[12] P.A. Nelson, S.H. Yoon, Estimation of acoustic source strength by inverse methods—Part I: conditioning of the inverse model, *Journal of Sound and Vibration* 233 (1999) 643–668.

[13] W. Neise, Review of fan noise generation mechanisms and control methods, *Proceedings of Fan Noise 92*, Senlis, France, 1992, pp. 45–56.

[14] G. Fournier, *Techniques de L'ingénieur*, *Traité de Sciences Fondamentales*, *A 430*. Aéroacoustique et hydroacoustique, 1990 (in French).

[15] A. Schumacher, J. Hald, K.B. Rasmussen, P.C. Hansen, Sound source reconstruction using inverse boundary element calculations, *Journal of the Acoustical Society of America* 113 (1) (2003) 114–127.

[16] T.V. Wood, S.M. Grace, Inverse aeroacoustic problem for a rectangular wing, *AIAA Journal* 38 (2) (2000) 203–210.

[17] W.K. Blake, *Mechanics of Flow Induced Sound and Vibration, Vol. 2, Complex Flow Structure Interactions*, Academic Press, New York, 1986.

[18] P.C. Hansen, *Rank-deficient and Discrete Ill-posed Problems*, SIAM, Philadephia, PA, 1998 247p.